

Exciton-Polariton Dynamics in Multilayered Materials

Saeed Rahmanian Koshkaki,^{1,*} Arshath Manjalingal,¹ Logan Blackham,¹ and Arkajit Mandal^{1,†}

¹*Department of Chemistry, Texas A&M University, College Station, Texas 77843, USA*

Coupling excitons with quantized radiation has been shown to enable coherent ballistic transport at room temperature inside optical cavities. Previous theoretical works employ a simple description of the material, depicting it as a single layer placed in the middle of the optical cavity, thereby ignoring the spatial variation of the radiation in the cavity quantization direction. In contrast, in most experiments, the optical cavity is filled with organic molecules or multilayered materials. Here, we develop an efficient mixed-quantum-classical approach, introducing a *bright layer* description, to simulate the exciton-polariton quantum dynamics. Our simulations reveal that, for the same Rabi splitting, a multilayer material extends the quantum coherence lifetime and enhances transport compared to a single-layer material. We find that this enhanced coherence can be traced to a synchronization of phonon fluctuations over multiple layers, wherein the collective light-matter coupling in a multilayered material effectively suppresses the phonon-induced dynamical disorder.

Introduction. Quantum coherence in the condensed phase typically lasts tens of femtoseconds at room temperature, due to phonon-induced decoherence intrinsic to the material itself [1]. Recent experiments have demonstrated that light-matter interaction inside optical cavities enables coherent quantum propagation of exciton-polaritons (EP) by effectively shielding polaritons from phonon fluctuations [2–8]. Specifically, prior theoretical works [2, 9–12], show that polaritons, which are part light and part matter, couple to phonons more weakly compared to bare excitons because only their matter component couples to the phonons, which is partly responsible for the sustained coherence lifetime of exciton-polaritons. In addition to this, our recent theoretical work suggests that the light-matter interactions approximately restore the phonon-induced translational symmetry breaking in materials [8]. Overall, these works reveal that coupling cavity radiation to materials provides tuning knobs for controlling phonon-induced decoherence beyond the traditional paradigms of material synthesis, paving the way for developing next-generation quantum devices [13, 14].

However, these theoretical works adopt a simplified model system that describes the material as a single layer placed at the center of the optical cavity (see Fig. 1a). This is in contrast to most of the experiments [2, 3, 5, 6, 15, 16] where the space between the reflective mirrors is filled with molecules or multiple layers of materials, as schematically illustrated in Fig. 1b. Consequently, the density of states in these two setups (i.e., multilayered vs. single-layered) are drastically different (see insets in Fig. 1c-d), with the multilayered material featuring an ensemble of optically dark bands that are absent in a single-layered material when coupled to cavity. Therefore, it is anticipated that the polariton quantum dynamics in these two setups will differ. However, the role of a multilayer configuration in polaritonic quantum dynamics has remained unexplored, which is the focus of this present work.

Simulating exciton-polariton dynamics in multilayered material is an extremely challenging task, as the number of required unit cells in a single layer exceeds $\sim 10^4$, thus requiring us to perform a quantum dynamics simulation involving $\sim 10^6$ states for $\sim 10^2$ layers, typical in these systems. To resolve this fundamental challenge, here we introduce an efficient mixed quantum-classical approach that uses a *bright-layer* description of the light-matter interaction and propagates the dynamics utilizing a split-operator approach. Using this convenient theoretical tool, we investigate the polaritonic quantum dynamics in multilayered materials. We discover a *phonon fluctuation synchronization effect* where the exciton-polaritons experience much lower phonon fluctuations and remain coherent for a longer time. We show that this effect originates from the delocalized nature of light-matter interactions, leading to an averaging of phonon fluctuations and suppression of phonon-induced

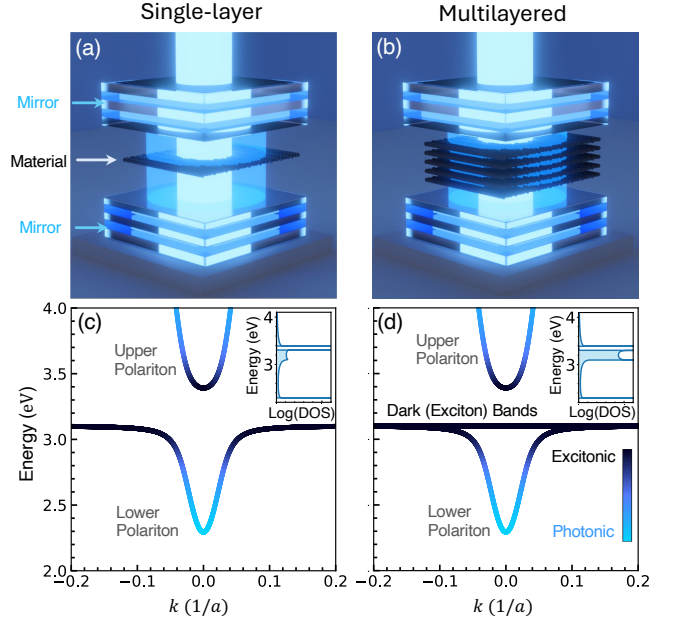


FIG. 1. **Schematics and band structures of single-layer vs. multilayer materials.** Illustration of (a) a single layer material and (b) multilayered material in an optical cavity, respectively. The exciton-polariton band structures of (c) single-layer and (d) multilayer materials in the absence of phonons ($\gamma = 0$). In a multilayer setup, in addition to the polariton bands, an ensemble of dark material bands exist. These dark bands increase the density of states (DOS) near the onsite energy value, which are plotted as insets within (c)-(d).

dynamic disorder. Here, we show that multilayered materials can extend the exciton-polariton coherence lifetime, up to an order of magnitude, and enhance exciton-polariton transport, which is relevant for developing polariton-based quantum devices [5, 14, 17].

Theory. To explore the dynamics of exciton-polaritons formed in multilayered materials, we consider a light-matter Hamiltonian beyond the long-wavelength approximation [7, 15, 18–20], which can be derived from the non-relativistic quantum electrodynamics Hamiltonian in the Coulomb gauge [15, 21], written as (in atomic units)

$$\hat{H}_{\text{LM}} = \hat{H}_{\text{ex}} + \hat{H}_{\text{phn}} + \hat{H}_{\text{cav}} + \hat{H}_{\text{ex-phn}} + \hat{H}_{\text{ex-cav}} + \hat{H}_{\text{loss}}, \quad (1)$$

where \hat{H}_{ex} , \hat{H}_{phn} and \hat{H}_{cav} are the bare excitonic, phonon, and cavity Hamiltonians, with $\hat{H}_{\text{ex-phn}}$ and $\hat{H}_{\text{ex-cav}}$ describing the

* rahmanian@tamu.edu

† mandal@tamu.edu

exciton-phonon and exciton-cavity interactions. Here, the last term \hat{H}_{loss} describes cavity photon loss. The bare excitonic Hamiltonian is written as

$$\hat{H}_{\text{ex}} = \sum_n \sum_m^M \left[\epsilon_0 \hat{X}_{n,m}^\dagger \hat{X}_{n,m} - \tau \left(\hat{X}_{n+1,m}^\dagger \hat{X}_{n,m} + h.c. \right) \right], \quad (2)$$

where $\hat{X}_{n,m}^\dagger$ creates an exciton at the site n in the m th layer, ϵ_0 is the onsite energy and τ is the hopping parameter. These layers are stacked parallel to each other with an interlayer spacing of $a_z = 4$ nm, with each site separated laterally by a distance of $a = 1.2$ nm, which corresponds to typical perovskite materials [22]. In this work, we also consider one phonon degree of freedom (DOF) per site, with the bare phonon Hamiltonian given by

$$\hat{H}_{\text{phn}} = \sum_{n,m} \left(\frac{\hat{p}_{n,m}^2}{2} + \frac{1}{2} \omega^2 \hat{q}_{n,m}^2 \right), \quad (3)$$

where $\hat{p}_{n,m}$ and $\hat{q}_{n,m}$ are the momentum and position of the phonons with frequency $\omega = 1440 \text{ cm}^{-1}$ [22]. We consider a typical form of the exciton-phonon coupling [2, 23–25] described by

$$\hat{H}_{\text{ex-phn}} = \gamma \sum_{n,m} \hat{q}_{n,m} \hat{X}_{n,m}^\dagger \hat{X}_{n,m}, \quad (4)$$

where γ is the exciton-phonon coupling strength. The bare cavity Hamiltonian \hat{H}_{cav} describes a set of confined radiation modes in a Fabry-Pérot optical cavity [7, 26–28] such that

$$\hat{H}_{\text{cav}} = \sum_{\mathbf{k}} \omega_{\mathbf{k}} \hat{a}_{\mathbf{k}}^\dagger \hat{a}_{\mathbf{k}}, \quad (5)$$

where $\hat{a}_{\mathbf{k}}^\dagger$ creates a photon of wavevector \mathbf{k} with a frequency $\omega_{\mathbf{k}} = \frac{c}{\eta} |\mathbf{k}|$ where c and $\eta = 2.4$ are the speed of light and the refractive index, respectively. In this work, we consider only two directions, i.e. x and y such that $\mathbf{k} = k_x \hat{x} + k_y \hat{y}$ with y as the cavity quantization direction. Similar to recent work [2, 9, 15, 20, 24, 29, 30] we impose a periodic boundary condition in the x direction, effectively quantizing the $k_x = \frac{2\pi n_x}{N \cdot a}$ where $n_x = 0, \pm 1, \pm 2, \dots$ and consider primary cavity mode along the y direction such that $k_y = \frac{\pi}{L}$ with $L = 1000 \text{ \AA}$ as the distance between the two reflective mirrors of the optical cavity. To simplify our notation, we denote $k = k_x$ and label all photonic operators and related parameters with k , as k_y is fixed, such that $\hat{H}_{\text{cav}} = \sum_{\mathbf{k}} \omega_{\mathbf{k}} \hat{a}_{\mathbf{k}}^\dagger \hat{a}_{\mathbf{k}} \rightarrow \sum_k \omega_k \hat{a}_k^\dagger \hat{a}_k$ and $\omega_k = \frac{c}{\eta} \sqrt{k_x^2 + k^2}$.

The light-matter interactions beyond the long-wavelength approximation [2, 24, 30, 31] is described by the $\hat{H}_{\text{ex-cav}}$ as

$$\hat{H}_{\text{ex-cav}} = \sum_{n,m,k} \frac{\Omega_k}{\sqrt{N}} \left(\hat{X}_{n,m}^\dagger \hat{a}_k e^{ikx_n} + h.c. \right) \sin(ky \cdot y_m), \quad (6)$$

where $\Omega_k = \sqrt{\frac{\omega_0}{\omega_k}} \Omega_0$ ($\Omega_0 = 480 \text{ meV}$ chosen here) is the light-matter coupling strength with the spatial location of the exciton $\hat{X}_{n,m}^\dagger$ as $R_{n,m} = x_n \hat{x} + y_m \hat{y}$. Finally, we model the cavity photon loss using a non-Hermitian Hamiltonian [20, 32–34]

$$\hat{H}_{\text{loss}} = -\frac{i}{2t_c} \sum_k \hat{a}_k^\dagger \hat{a}_k, \quad (7)$$

where t_c is the cavity photon lifetime.

Quantum Dynamical Approach. In this work, we employ a custom mixed-quantum-classical method based on the mean-field Ehrenfest approach to simulate the dynamics of the light-matter hybrid system. Within the standard Ehrenfest approach, that has been extensively used to simulate non-adiabatic dynamics of polaritons, [7, 9, 10, 20, 35–38] the nuclear (or slow) degree of freedom is evolved classically, with $\{\hat{q}_{n,m}, \hat{p}_{n,m}\} \rightarrow \{q_{n,m}, p_{n,m}\}$, following the Hamiltonian's equation of motion,

$$\dot{p}_{n,m}(t) = -\left\langle \Psi(t) \left| \frac{d\hat{H}_{\text{LM}}}{dq_{n,m}} \right| \Psi(t) \right\rangle, \quad \dot{q}_{n,m}(t) = p_{n,m}(t), \quad (8)$$

where $|\Psi(t)\rangle$ is the electronic-photonic wavefunction at time t . The electronic-photonic wavefunction is evolved using the time-dependent Schrödinger equation written as

$$i|\dot{\Psi}(t)\rangle = \left[\hat{H}_{\text{LM}} - \frac{1}{2} \sum_{n,m} \frac{p_{n,m}^2}{2} \right] |\Psi(t)\rangle. \quad (9)$$

In this work, we confine the exciton-polariton dynamics to the single excited subspace, such that

$$\begin{aligned} |\Psi(t)\rangle &= \left(\sum_k c_k(t) \hat{a}_k^\dagger + \sum_{n,m} b_{n,m}(t) \hat{X}_{n,m}^\dagger \right) |\bar{0}\rangle \\ &\equiv \sum_k c_k(t) |1_k\rangle + \sum_{n,m} b_{n,m}(t) |n,m\rangle \end{aligned} \quad (10)$$

where $c_k(t)$ and $b_{n,m}(t)$ are time-dependent coefficients. In the second line, we have introduced the compact representation $|1_k\rangle \equiv \hat{a}_k^\dagger |\bar{0}\rangle$ and $|n,m\rangle \equiv \hat{X}_{n,m}^\dagger |\bar{0}\rangle$, with $|\bar{0}\rangle$ as the ground (or vacuum) state of the system, for simplicity. Despite the mixed quantum-classical treatment of the full light-matter Hamiltonian, numerically solving Eq. 9 is extremely challenging as the present work requires a basis of size $\sim 10^6$. To resolve this issue, we develop a *split-operator* approach where a short-time (a single time-step) propagation of $|\Psi(t)\rangle$ is obtained as

$$\begin{aligned} |\Psi(t + \delta t)\rangle &= e^{-i\hat{H}_{\text{LM}}\delta t} |\Psi(t)\rangle \\ &\approx \hat{U}_{\text{ft}} \hat{U}_{\text{B}} \left(\hat{U}_{\text{B}}^\dagger \hat{U}_{\text{ft}}^\dagger e^{-i\hat{H}_{\text{EP}}\delta t} \hat{U}_{\text{ft}} \hat{U}_{\text{B}} \right) \hat{U}_{\text{B}}^\dagger \hat{U}_{\text{ft}}^\dagger e^{-i\hat{H}_{\text{env}}\delta t} |\Psi(t)\rangle \\ &= \hat{U}_{\text{ft}} \hat{U}_{\text{B}} \cdot e^{-i(\hat{U}_{\text{B}}^\dagger \hat{U}_{\text{ft}}^\dagger \hat{H}_{\text{EP}} \hat{U}_{\text{ft}} \hat{U}_{\text{B}})\delta t} \cdot \hat{U}_{\text{B}}^\dagger \hat{U}_{\text{ft}}^\dagger \cdot e^{-i\hat{H}_{\text{env}}\delta t} |\Psi(t)\rangle, \end{aligned} \quad (12)$$

where $\hat{H}_{\text{LM}} = \hat{H}_{\text{EP}} + \hat{H}_{\text{env}}$ with $\hat{H}_{\text{env}} = \hat{H}_{\text{phn}} + \hat{H}_{\text{ex-phn}} + \hat{H}_{\text{loss}}$ and $\hat{H}_{\text{EP}} = \hat{H}_{\text{ex}} + \hat{H}_{\text{cav}} + \hat{H}_{\text{ex-cav}}$. Here \hat{H}_{env} is the diagonal in the exciton-photon basis $\{|1_k\rangle, |n,m\rangle\}$ chosen here. As a result, the action of the matrix $e^{-i\hat{H}_{\text{env}}\delta t}$ on the vector $|\Psi(t)\rangle$ reduces to a simple Hadamard product between a vector containing the diagonal elements of $e^{-i\hat{H}_{\text{env}}\delta t}$ and $|\Psi(t)\rangle$. Meanwhile, \hat{U}_{ft} is a unitary operator that Fourier transforms the excitonic subspace within each layer, such that $\hat{U}_{\text{ft}} |\Psi(t)\rangle = \sum_k c_k(t) |1_k\rangle + \hat{U}_{\text{ft}} \sum_{n,m} b_{n,m}(t) |n,m\rangle = \sum_k c_k(t) |1_k\rangle + \sum_{k,m} b_{k,m}(t) |k,m\rangle$. We perform this Fourier transformation using the Fast Fourier Transformation (FFT) algorithm, which scales as $N \log N$ resulting in a significant reduction of the computation cost [29, 39, 40]. Importantly, here we introduce the unitary operator $\hat{U}_{\text{B}} = \hat{U}_{\text{D}} \cdot \hat{U}_{\text{db}}$, where \hat{U}_{db} transforms the excitonic subspace into a *dark-bright* layers subspace [15] and \hat{U}_{D} diagonalizes this transformed exciton-polariton Hamiltonian,

$$\begin{aligned} \hat{U}_{\text{B}}^\dagger \hat{U}_{\text{ft}}^\dagger \hat{H}_{\text{EP}} \hat{U}_{\text{ft}} \hat{U}_{\text{B}} &= \hat{U}_{\text{B}}^\dagger \left[\hat{U}_{\text{ft}}^\dagger (\hat{H}_{\text{ex}} + \hat{H}_{\text{ex-cav}}) \hat{U}_{\text{ft}} + \hat{H}_{\text{cav}} \right] \hat{U}_{\text{B}} \\ &= \hat{U}_{\text{D}}^\dagger \sum_k \left[\epsilon_k \hat{X}_{k,b}^\dagger \hat{X}_{k,b} + \sqrt{S} \Omega_k \left(\hat{X}_{k,b}^\dagger \hat{a}_k + h.c. \right) \right. \\ &\quad \left. + \omega_k \hat{a}_k^\dagger \hat{a}_k \right] \hat{U}_{\text{D}} + \sum_{k,d} \epsilon_k \hat{X}_{k,d}^\dagger \hat{X}_{k,d} \\ &= \sum_{k,i \in \{\pm\}} \omega_{k,i} \hat{P}_{k,i}^\dagger \hat{P}_{k,i} + \sum_{k,d} \epsilon_k \hat{X}_{k,d}^\dagger \hat{X}_{k,d} \end{aligned} \quad (14)$$

where $\hat{X}_{k,b}^\dagger = \frac{1}{\sqrt{S}} \sum_m \sin(k \cdot y_m) \hat{X}_{k,m}^\dagger$ are bright layer exciton operators, with the normalization constant $S = \sum_m \sin^2(k \cdot y_m)$. Here, $\hat{X}_{k,b}^\dagger$ creates an exciton delocalized over all layers with an in-plane wavevector k . On the other hand, $\hat{X}_{k,d}^\dagger = \sum_m s_{m,d} \hat{X}_{k,m}^\dagger$, with $\sum_m s_{m,d}^2 = 1$ and $\sum_m s_{m,d} \cdot \sin(k \cdot y_m) = 0$, are dark layers exciton operators that do not couple to cavity radiation modes. These dark exciton operators form dark exciton bands, which are illustrated in Fig. 1d. In the last line of Eq. 13, we have introduced the upper and lower polariton operators,

$$\hat{P}_{k,+}^\dagger = \sin \theta_k \cdot \hat{a}_k^\dagger + \cos \theta_k \cdot \hat{X}_{k,b}^\dagger \quad (15)$$

$$\hat{P}_{k,-}^\dagger = \cos \theta_k \cdot \hat{a}_k^\dagger - \sin \theta_k \cdot \hat{X}_{k,b}^\dagger \quad (16)$$

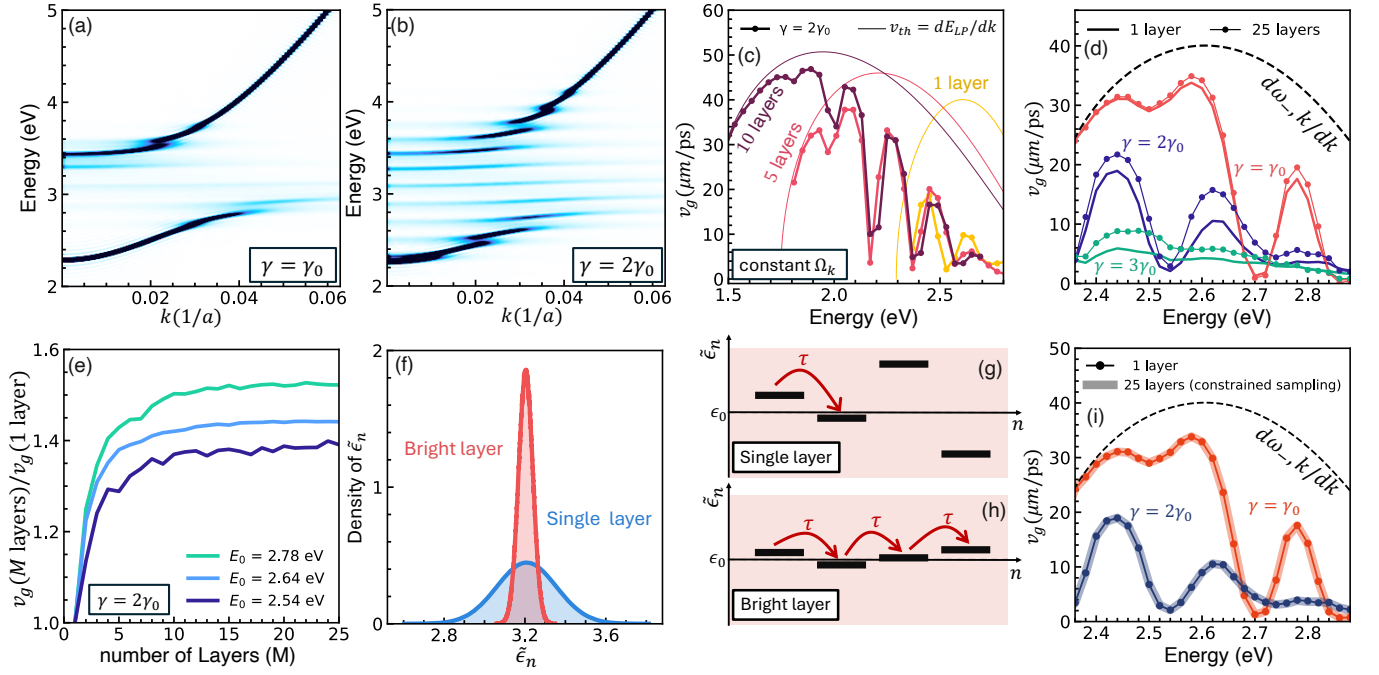


FIG. 2. **Exciton-polariton dynamics and spectra in multilayered materials ($M = 25$) and the phonon fluctuation synchronization effect.** The exciton-polariton angle-resolved spectra at (a) $\gamma = \gamma_0$ and (b) $\gamma = 2\gamma_0$. Exciton-polariton group velocity computed from quantum dynamical simulations vs. theoretical curve with (c) light-matter coupling per layer Ω_k a constant and (d) the total Rabi-splitting $\sqrt{S}\Omega_k$ a constant. Here the phonon coupling γ is written in terms of γ_0 , a constant. (e) The ratio of group velocities in multilayered material to a single-layer material. (f) Distribution of on-site excitonic energy. Illustration of hopping dynamics in (g) a single-layer material with higher disorder and (h) in a multilayered material with effectively lower disorder. (i) Group velocity in single-layered and multilayered material with constrained sampling of $q_{n,m}(t=0) = q_{n,1}(t=0)$. ($\gamma_0 \approx 5.8 \times 10^{-4}$ a.u.)

where $\theta_k = \frac{1}{2} \tan^{-1}[2\sqrt{S}\Omega_k/(\omega_k - \epsilon_k)]$ is a light-matter mixing angle [7, 41]. This diagonal form allows us to propagate the exciton polariton Hamiltonian in an efficient manner. Finally, an expectation value of an operator \hat{A} is computed as $\langle \hat{A} \rangle \approx \langle \langle \Psi(t) | \hat{A} | \Psi(t) \rangle \rangle_{\text{MFE}}$ where $\langle \dots \rangle_{\text{MFE}}$ indicates averaging over trajectories generated from the initial realizations of nuclear coordinates $\{q_{n,m}(0), p_{n,m}(0)\}$. Details of our propagation scheme are provided in the Supplementary Information (SI).

Results and Discussion. Here we model the exciton-phonon part of the system based on a multilayered perovskite material [22], which has on-site energy $\epsilon_0 = 3.2$ eV, a phonon frequency of $\omega = 1440$ cm^{-1} and a hopping parameter of $\tau = 400$ cm^{-1} with an interlayer spacing of 4 nm and a lattice spacing of $a = 1.2$ nm. However, the conclusions of this work are generic and is applicable to a wide variety of organic and inorganic exciton-polaritons. Further details of the parameters used in this work are provided in the SI.

Fig. 2a-b present the angle-resolved polariton spectra computed using our quantum dynamical approach (see details in the SI) for a single-layer material coupled to cavity radiation modes. The theoretical polariton dispersion curves presented in Fig. 1c, which are obtained by diagonalizing \hat{H}_{EP} (see Eq. 13), feature smooth polariton curves, as expected. In contrast, phonon interaction with the exciton-polaritons introduces vibronic structure to the polariton dispersion, as can be seen in Fig. 2a. Increase in the phonon coupling $\gamma = 2\gamma_0$ (where $\gamma_0 = 1.1\sqrt{\omega^3}$), in Fig. 2b makes the vibronic structure more prominent. The existence of these vibronic bands and their relation to phonon coupling γ can be, very crudely, explained due to the Franck-Condon overlaps between displaced harmonic oscillator states of the phonons. In our recent work [8], we have presented a microscopic theory, where these successive vibronic bands describe excitations to a phonon field, which provides a quantitatively accurate description.

Importantly, the vibronic structure in polariton dispersion directly shows up in the group velocities obtained via direct quantum dynamics simulations. In our quantum dynamics simulations, we model a resonant excitation in the lower polariton at the energy E_0 by selecting an exciton-polariton wavefunction $|\Psi(0)\rangle = \sum_{k \in \mathcal{E}_{\text{exc}}} \tilde{c}_k \hat{P}_{k,-}^\dagger |\bar{0}\rangle$, which is energetically localized within an energy window \mathcal{E}_{exc} (set to be 50 meV around E_0). We choose the coefficients \tilde{c}_k via a Monte Carlo approach (see SI) to ensure that $|\Psi(0)\rangle$ is also spatially localized at the center in the plane of the materials (in the \vec{x} direction).

Fig. 2c-d presents the group velocities extracted from the time-dependent excitonic density $\langle \Psi(t) | \hat{X}_{n,m}^\dagger \hat{X}_{n,m} | \Psi(t) \rangle$ at short times ($t < 300$ fs) with different numbers of layers of the material coupled to the cavity radiation. In Fig. 2c we keep each layer's coupling to the radiation Ω_k a constant. As a result, the overall Rabi-splitting $\sqrt{S}\Omega_k$ roughly scales with $\sim \sqrt{M}$ where M is the number of layers. The group velocities obtained numerically (solid lines with filled circles) show an oscillatory pattern due to the presence of the vibronic structure in the exciton-polariton dispersion. An increase in the number of layers, from $M = 1$ (yellow) to $M = 5$ (light red), and $M = 10$ (dark red), leads to an overall redshift due to the increase in the Rabi-splitting. Notably, the computed group velocities are much smaller (renormalized) than the theoretical group velocity $\frac{d}{dk}\omega_{-,k}$ (i.e. slope of the dispersion) in bare exciton-polariton. This renormalization effect has been observed in multiple recent experiments [2, 3, 6]. To clearly analyze the role of multiple layers in the exciton-polariton dynamics, in Fig. 2d and the rest of the results presented in this work we keep $\sqrt{S}\Omega_k$ a constant.

Fig. 2d presents the exciton-polariton group velocities in a multilayered material (with $M = 25$) compared to a single-layered material at various phonon couplings. Fig. 2d reveals that for the same effective Rabi splitting, $\sqrt{S}\Omega_k$, the exciton-polariton group veloc-

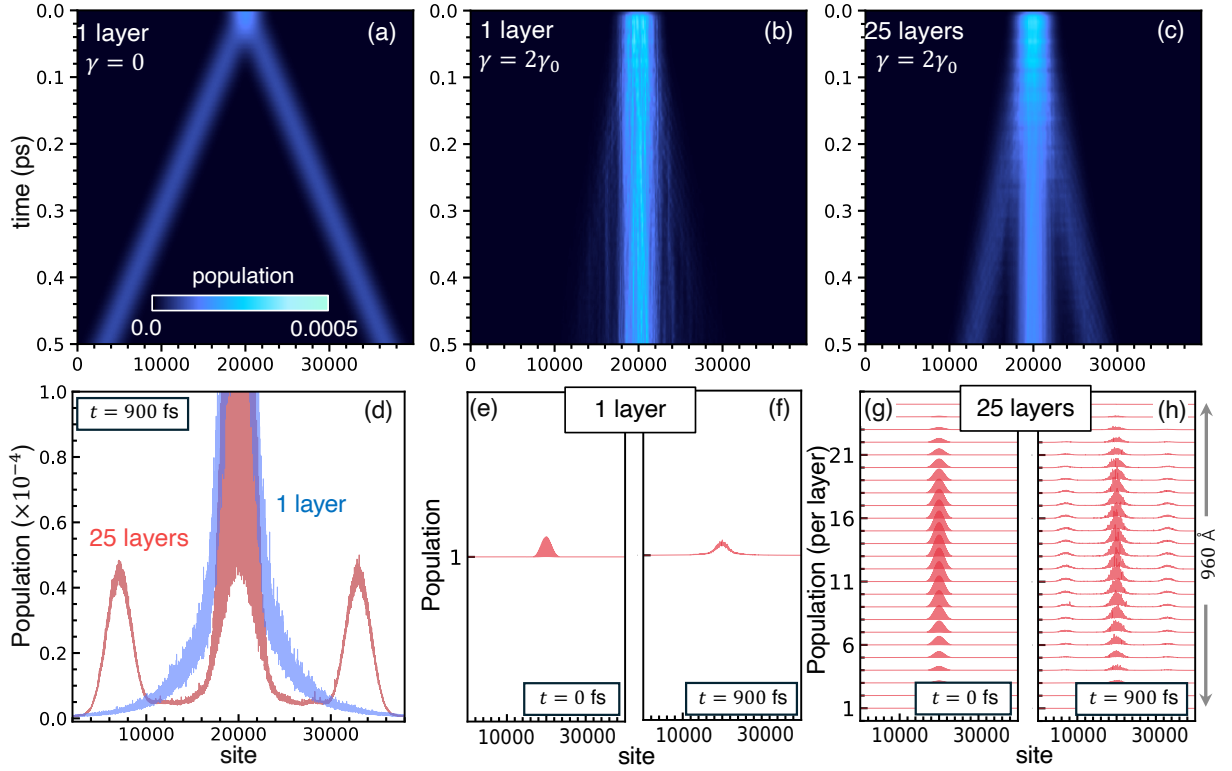


FIG. 3. Comparing exciton-polariton dynamics in single-layer vs. multilayered materials ($M = 25$) with the initial excitation at $E_0 = 2.64$ eV. (a) Time-dependent exciton-polariton density for a single-layer material with no phonon couplings, i.e. $\gamma = 0$. (b)-(c) Same as (a) but in the presence of phonon couplings $\gamma = 2\gamma_0$ in (b) a single and (c) multilayered material. (d) Site-resolved exciton density at $t = 900$ fs and $\gamma = 2\gamma_0$. To determine the multilayer exciton populations in (d), we summed the density contributions from all layers at each site. (e)-(h) Site and layer-resolved exciton density for (e)-(f) a single layer and (g)-(h) multilayered material at $t = 0$ and $t = 900$ fs with the same parameters as in (d). ($\gamma_0 \approx 5.8 \times 10^{-4}$ a.u.)

ity in a multilayered material could be substantially higher than the single-layered material. This is further illustrated in Fig. 2e which presents the enhancement of group velocity as a function of the number of layers placed inside an optical cavity. We find that the exciton-polariton density in multilayered material can propagate with velocities upwards of $\sim 50\%$ higher than in a single-layer material.

This is surprising because the number of phonon modes interacting with the exciton-polariton subsystem is significantly higher in a multilayered material compared to a single-layer material. However, despite the increase in the number of phonon modes, which one expects to provide additional sources of dissipation and fluctuation, the exciton-polariton propagates faster with a longer decoherence time. We find that this effect originates from a synchronization of phonon fluctuations in the collective bright layer leading to the suppression of phonon-induced decoherence and enhanced group velocity.

Phonon fluctuation synchronization effect. To provide a microscopic understanding of this effect, we analyze the term $\hat{H}_{\text{ex-phn}}$ in the light-matter Hamiltonian. We introduce the bright exciton operators in real space, defined as $\hat{X}_{n,b}^\dagger = \frac{1}{\sqrt{S}} \sum_m \sin(k_y \cdot y_m) \hat{X}_{n,m}^\dagger = \frac{1}{\sqrt{N}} \sum_n \hat{X}_{k,b}^\dagger e^{-ik \cdot x_n}$. Since only the bright exciton operators $\{\hat{X}_{n,b}^\dagger\} \equiv \{\hat{X}_{k,b}^\dagger\}$ directly contribute (see Eq. 13) in the dynamics of the exciton-polaritons, we focus on the exciton-phonon coupling term in the subspace defined by the projection operator $\mathcal{P} = \sum_n \hat{X}_{n,b}^\dagger \hat{X}_{n,b} = \sum_n |n, b\rangle \langle n, b|$, which is

written as

$$\begin{aligned} \mathcal{P} \left(\hat{H}_{\text{ex-phn}} \right) \mathcal{P} &= \gamma \sum_n \hat{X}_{n,b}^\dagger \hat{X}_{n,b} \left(\frac{1}{S} \sum_m q_{n,m} \sin^2(k \cdot y_m) \right) \\ &= \gamma \sum_n \hat{X}_{n,b}^\dagger \hat{X}_{n,b} \tilde{q}_n, \end{aligned} \quad (17)$$

where $\tilde{q}_n = \frac{1}{S} \sum_m q_{n,m} \sin^2(k \cdot y_m)$. Therefore, exciton-polariton dynamics effectively interact with the collective phonons \tilde{q}_n that are delocalized over all the layers. Importantly, the \tilde{q}_n distribution is much narrower than the distribution of $q_{n,m}$ effectively exhibiting a phonon fluctuation synchronization in multilayered materials. This phonon fluctuation synchronization can also be viewed as an effective reduction in temperature (shrinking the thermal distribution of the phonons) leading to enhanced coherent transport of exciton-polaritons.

Fig. 2f presents the distribution of the excitonic on-site energy compared to the multilayered material. Due to the fluctuation synchronization discussed above, the fluctuations in the effective excitonic on-site energy $\tilde{\epsilon}_n = \epsilon_0 + \gamma \tilde{q}_n$ in the collective bright layer is much less compared to the on-site energies $\epsilon_n = \epsilon_0 + \gamma q_n$ in the single-layer scenario. As a result, the exciton-polariton propagation is enhanced as hopping between neighboring sites is easier, which is schematically illustrated in Fig. 2g-h.

To test our phonon fluctuation synchronization hypothesis, in Fig. 2i, we perform quantum dynamical simulations in multilayered materials by sampling the phonons in a constrained fashion, i.e. $q_{n,m}(t=0) = q_{n,1}(t=0)$, such that the initial position of a phonon at a site n is the same regardless of the layer. As a result, $\tilde{q}_n = q_{n,1}$, which means that the fluctuations experienced by

the collective bright layer in a multilayered material is the same as in the single-layer material. The group velocities presented in Fig. 2i show that the dynamics of the multilayered material under constrained sampling are identical to the single-layer material, corroborating our phonon fluctuation synchronization hypothesis.

Fig. 3 presents time-dependent exciton-polariton density (exciton population at each site n) to illustrate how the phonon fluctuation synchronization in multilayered materials can enable coherent transport. Fig. 3a presents the time-dependent exciton population in a single-layer material in the absence of phonon ($\gamma = 0$). As expected, the exciton-polariton population, initially prepared at the center, propagates ballistically. In the presence of strong phonon interaction ($\gamma \neq 0$) the exciton-polariton propagation in a single-layer material, presented in Fig. 3b, appears incoherent, exhibiting diffusive transport. In contrast, the exciton-polariton transport in multilayered material at the same exciton-phonon coupling γ , presented in Fig. 3c, shows ballistic coherent propagation of the exciton-polariton wavefront. This remarkable effect can be clearly seen in Fig. 3d which presents the exciton-polariton density at $t = 900$ fs. We see that the wavefront in multilayered material propagates coherently, which is missing in the single-layer case.

Fig. 3g-h further illustrates that the exciton-polariton wavefront is delocalized over all the layers, with Fig. 3e-f presenting the corresponding results in the single-layer scenario. This shows how delocalization of exciton-polariton density in the transverse direction exhibits enhanced transport in the longitudinal direction (or in the plane of the material). We find that this phonon fluctuation synchronization effect is quite ubiquitous, showing up in a wide range of parameter regimes. We present more exciton density propagation data for different values of E_0 and γ in the SI.

Fig. 4a-b presents the excitonic mean square displacement (MSD) for an initially prepared exciton-polariton at an energy window of 2.64 ± 0.025 eV. The excitonic MSD is computed as [2, 9, 29]

$$\text{MSD} = a^2 \left(\sum_n n^2 P_n(t) - \left(\sum_n n P_n(t) \right)^2 \right), \quad (18)$$

where $P_n(t) = \left\langle \frac{1}{\mathcal{N}} \langle \Psi(t) | \hat{X}_n^\dagger \hat{X}_n | \Psi(t) \rangle \right\rangle_{\text{MFE}}$ is excitonic density at the site n with $\mathcal{N} = \sum_n \langle \Psi(t) | \hat{X}_n^\dagger \hat{X}_n | \Psi(t) \rangle$ a normalization constant. In the absence of phonons ($\gamma = 0$), MSD is quadratic (dark blue line in Fig. 4a) in time, i.e. ballistic, as expected. In the presence of phonon interactions, ($\gamma \neq 0$) MSD is quadratic till ~ 300 fs and becomes almost linear beyond this time, thereby exhibiting diffusive transport as phonon-induced decoherence sets in. For the same phonon coupling, the MSD appears to be ballistic for a longer time in the case of multilayered material, suggestive of extended coherence lifetime due to the phonon fluctuation synchronization discussed above. Clearly the MSD reaches a higher value in the case of a multilayered material compared to a single-layer material.

Fig. 4b presents MSD in the presence of cavity loss that accounts for the finite lifetime of a photon trapped inside an imperfect optical cavity. Overall, the trends are the same as in Fig. 4a but with an overall lower MSD. These results agree with recent theoretical and experimental works which demonstrate that MSD is suppressed in the presence of cavity loss [6, 9, 29].

While ballistic transport is suggestive of coherent dynamics, it only provides indirect evidence of decoherence suppression. To provide a quantitative measure and a direct confirmation of decoherence suppression, we compute the purity [42–44] which is defined as $\text{Tr}[\hat{\rho}_{\text{EP}}^2(t)]$ where $\hat{\rho}_{\text{EP}}(t)$ is the reduced density matrix describing the exciton-polariton subsystem. Within our mixed-quantum classical simulations, the exciton-polariton reduced density matrix is computed as $\langle |\Psi(t)\rangle \langle \Psi(t)| \rangle_{\text{MFE}}$. In the SI we provide an efficient approach to computing the purity in our mixed-quantum-classical simulations.

Fig. 4c-d presents the time-dependent purity $\text{Tr}[\hat{\rho}_{\text{EP}}^2(t)]$ at two different windows of initial excitation $E_0 = 2.58$ and 2.78 eV. In the single-layer scenario (violet solid line), at times $t = 0$ the purity

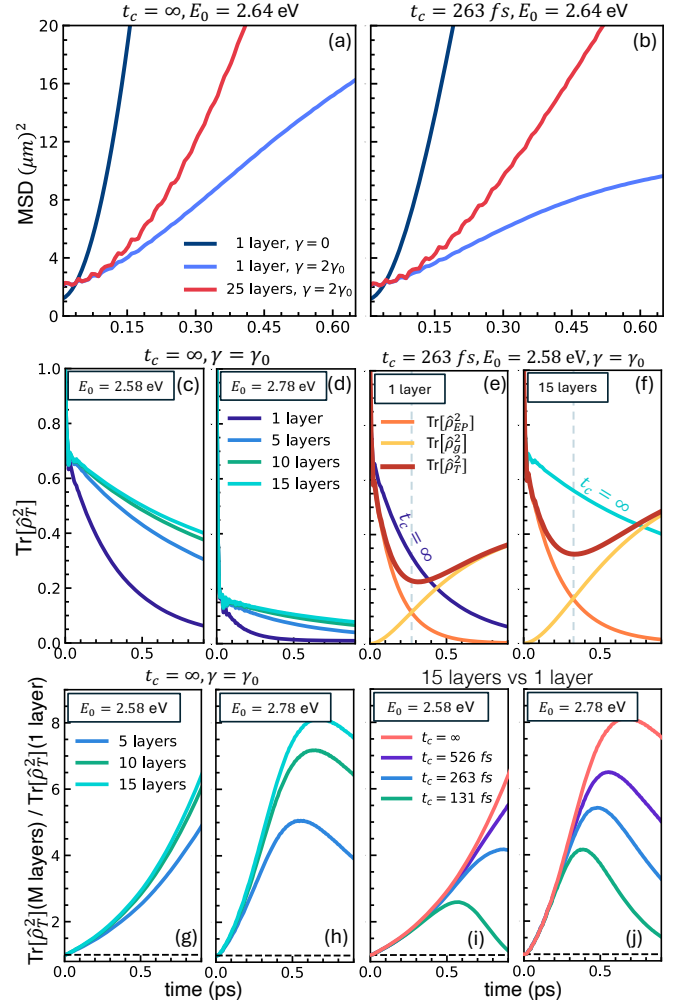


FIG. 4. **Effect of cavity photon loss on mean-square displacement (MSD) and purity in multilayered materials.** MSD in single-layer material vs. multilayered material ($M = 25$) (a) in the absence ($t_c = \infty$) and (b) presence ($t_c = 263$ fs) of cavity photon loss. Purity in the absence of photon loss for different number of layers (M) and the initial excitation at (c) $E_0 = 2.58$ eV and (d) $E_0 = 2.78$ eV. Total purity ($\text{Tr}[\hat{\rho}_{\text{T}}^2(t)]$) along with exciton-polariton ($\text{Tr}[\hat{\rho}_{\text{EP}}^2(t)]$) and ground state ($\text{Tr}[\hat{\rho}_{\text{G}}^2(t)]$) contributions to total purity in the presence of cavity photon loss ($t_c = 263$ fs) and initial excitation at $E_0 = 2.58$ eV for (e) single layer and (f) 15 layers. The ratio of the purity of multilayered materials ($M > 1$) relative to the purity of single-layer material ($M = 1$) with no cavity loss and initial excitation at (g) $E_0 = 2.58$ eV and (h) $E_0 = 2.78$ eV. The ratio of exciton-polariton purity of 15-layer material relative to the single-layer material for different cavity photon lifetimes and initial excitation at (i) $E_0 = 2.58$ eV and (j) $E_0 = 2.78$ eV. ($\gamma_0 \approx 5.8 \times 10^{-4}$ a.u.)

is one, which indicates a pure (coherent) state. At longer times, $\sim t = 600$ fs the purity decays toward zero, indicating phonon-induced decoherence of the exciton-polariton subsystem. Fig. 4c-d, shows that an increase in the number of layers significantly suppresses the decay of the purity, directly depicting an extended coherence lifetime in multilayered materials. Overall, we find that multilayered materials can enhance purity by up to a factor of ~ 8 as shown in Fig. 4g-h which presents the ratio of purity in a multilayered material to a single-layer material.

Fig. 4e-f presents the time-dependent purity in the presence of

cavity loss. Note that in the presence of cavity loss, the population in the exciton-photon subspace $\{|1_k\rangle, |n, m\rangle\}$ leaks out to the ground state $|\bar{0}\rangle$. As a result, the total reduced density matrix (when tracing over the phonon degree of freedom) can be defined as $\hat{\rho}_T(t) = \hat{\rho}_{EP}(t) + \hat{\rho}_g(t) = \sum_{\alpha, \beta} \rho_{\alpha\beta}(t) |\alpha\rangle\langle\beta| + \rho_{gg}(t) |\bar{0}\rangle\langle\bar{0}|$ where $\{|\alpha\rangle, |\beta\rangle\} \in \{|1_k\rangle, |n, m\rangle\}$. As a result, the total purity can be written down as

$$\text{Tr}[\hat{\rho}_T^2(t)] = \text{Tr}[\hat{\rho}_{EP}^2(t)] + \text{Tr}[\hat{\rho}_g^2(t)]. \quad (19)$$

These three quantities, $\text{Tr}[\hat{\rho}_T^2(t)]$, $\text{Tr}[\hat{\rho}_{EP}^2(t)]$, and $\text{Tr}[\hat{\rho}_g^2(t)] = \rho_{gg}^2(t)$, are presented in Fig. 4e-f at a cavity photon lifetime $t_c = 263$ fs. Note that at $t \gg t_c$ the total purity reaches 1 because the total density matrix $\hat{\rho}_T(t \gg t_c) \rightarrow |\bar{0}\rangle\langle\bar{0}|$ which is a pure state. At the same time, the coherence in the exciton-polariton subspace becomes zero with $\hat{\rho}_{EP} \rightarrow 0$. Overall the total purity (red solid line) decays till 250 fs primarily due to the decay of exciton polariton purity $\text{Tr}[\hat{\rho}_{EP}^2(t)]$. The rise in the total purity after 400 fs is due to the increase in $\rho_{gg}^2(t)$ as the population leaks to the ground state. Comparing to the no cavity loss scenario, represented by the violet and cyan solid line in Fig. 4e-f respectively, the $\text{Tr}[\hat{\rho}_{EP}^2(t)]$ decays faster, which is due to the loss in the total population in the exciton-polariton subspace. Importantly, regardless of the presence or absence of cavity loss, the multilayered material suppresses the decay in exciton-polariton purity.

This is further illustrated in Fig. 4i-j which presents the ratio of the purity in the multilayered to the single-layered scenario. We find that an increase in cavity loss suppresses the multilayer protection of coherence. This is expected as the phonon fluctuation synchronization effect in the multilayered materials only protects against phonon-induced decoherence and does not directly combat cavity loss. However, we find that even in a very lossy scenario ($t_c = 131$ fs) multilayered materials can enhance purity by a factor of ~ 4 .

Other parameter regimes. Overall, we find that the phonon fluctuation synchronization effect exists in a wide range of cavity setups. In the main text, we present two additional parameter regimes: (a) low photon frequency $\omega = 720 \text{ cm}^{-1}$ and (b) low light-matter coupling regime with $\Omega_0 = 240 \text{ meV}$.

Fig. 5 presents group velocity and exciton population density at $t = 700$ fs (for the yellow-circled point in group velocity data) of single-layer and multilayered material (with $M=25$). In Fig. 5a-b, we use phonon frequency to $\omega = 720 \text{ cm}^{-1}$ ($\gamma_0 = 1.1\sqrt{\omega^3}$). Just as the result presented above, Fig. 5a shows an enhancement in group velocity (over $\sim 50\%$) in multilayered materials compared to the single-layer case. Similarly, Fig. 5b shows that the exciton population density in multilayered materials exhibits a coherently propagating wavefront, which is absent in the single-layer case. In Fig. 5c-d, we set the exciton-photon coupling to $\Omega_0 = 240 \text{ meV}$. For this parameter, Fig. 5c shows that the group velocity enhancement in multilayered materials, compared to single-layer materials, is small but still noticeable. However, Fig. 5d demonstrates that, for this exciton-photon coupling, exciton population density in the multilayer material propagates more coherently. The population density in the multilayered material are less noisy, and the population around the central site is more localized. The results for these two sets of parameters show that the coherence enhancement for the multilayered materials is a generic effect. However, having a larger exciton-photon coupling makes this enhancement more prominent.

Conclusion. In this work, we have studied the exciton-polariton dynamics in multilayer materials and compared their transport and coherence to single-layer materials. To achieve this, we introduced a new, fast, and highly efficient mixed quantum-classical approach that utilizes a *bright layer* description of the light-matter interactions, allowing us to simulate a large number of quantum states ($\sim 10^6$).

Using our quantum dynamics approach, we found a phonon fluctuation synchronization effect where the delocalized light-matter interactions in a multilayered material shield exciton-polaritons from phonon-induced decoherence. As a result, exciton-polaritons

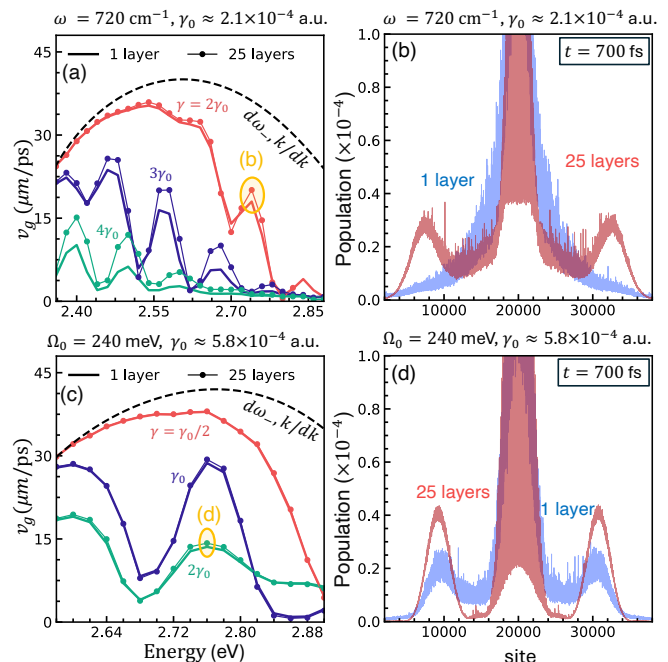


FIG. 5. **Exciton-polariton dynamics in multilayered materials ($M = 25$) at various parameter regimes.** (a)-(b) exciton-polariton dynamics at photon frequency $\omega = 720 \text{ cm}^{-1}$ ($\gamma_0 \approx 2.1 \times 10^{-4}$ a.u.) with the rest of the parameters the same as Fig. 2d. (a) Exciton-polariton group velocity computed from quantum dynamical simulations vs. theoretical curve and (b) site-resolved exciton density at $t = 700$ fs for yellow-circled point in (a). (c)-(d) Same as (a)-(b) but with light-matter coupling $\Omega_0 = 240 \text{ meV}$ and $\omega = 1440 \text{ cm}^{-1}$ ($\gamma_0 \approx 5.8 \times 10^{-4}$ a.u.).

propagate faster with an increased group velocity and, *more importantly*, remain more coherent for a longer time in multilayered materials despite interacting with a significantly larger number of phonon modes. We show that this phonon fluctuation synchronization effect originates from a fluctuation averaging in the transverse direction (perpendicular to the mirror plane) over multiple layers that suppresses dynamic disorder in the longitudinal direction (in the plane of the materials/mirrors) enhancing transport in the material plane. Our analytical analysis reveal that only one effective layer (the bright layer) couples with the cavity modes, while the rest remain uncoupled (dark layers). It is this bright layer, delocalized over all layers, that experiences lesser phonon fluctuations than in a single-layer material. We also show that even in the presence of cavity loss, multilayered material enhances transport and coherence, although to a lesser extent. We show such enhancement also exists in other parameter regimes, such as at lower phonon frequency or at lower light-matter coupling strength.

Our work provides microscopic insights into exciton-polariton dynamics in multilayered materials and illustrates that quantum coherence lifetime can be extended by using multilayered cavity architecture. This work reveals that the pathway to polariton quantum devices is likely via stacked multilayered materials.

I. DATA AVAILABILITY

The data that support the plots within this paper and other findings of this study are available from the corresponding authors upon a reasonable request.

II. CODE AVAILABILITY

The source code that supports the findings of this study is available from the corresponding author upon reasonable request.

III. ACKNOWLEDGMENTS

This work was supported by the Texas A&M startup funds. This work used TAMU FASTER at the Texas A&M University through allocation PHY230021 from the Advanced Cyberinfrastructure Coordination Ecosystem: Services & Support (ACCESS) program, which is supported by National Science Foundation grants #2138259, #2138286, #2138307, #2137603, and #2138296. A.M. appreciates inspiring discussions with Yi Rao,

Milan Delor, Daniel Tabor, Dong Hee Son, Pengfei Huo, David R. Reichman, Pritha Ghosh, and Sachith Wickramasinghe.

IV. AUTHOR CONTRIBUTIONS

S. R. K. and A. M. designed the research. S. R. K., L. B. and A. M. (Arshath Manjalingal) developed the quantum dynamical approach. and analyzed data. S. R. K. performed the quantum dynamical simulations. S. R. K., L. B. and A. M. (Arshath Manjalingal) and A. M. analyzed data and wrote the manuscript.

V. COMPETING INTERESTS

The authors declare no competing interests.

-
- [1] Nitzan, A. *Chemical Dynamics in Condensed Phases: Relaxation, Transfer and Reactions in Condensed Molecular Systems* (Oxford University Press: Oxford, U.K., 2006).
- [2] Xu, D. *et al.* Ultrafast imaging of polariton propagation and interactions. *Nature Communications* **14**, 3881 (2023).
- [3] Balasubrahmaniyam, M. *et al.* From enhanced diffusion to ultrafast ballistic motion of hybrid light–matter excitations. *Nature Materials* **22**, 338–344 (2023).
- [4] Keeling, J. & Turnbull, G. See how they run. *Nature Materials* **22**, 276–277 (2023).
- [5] Sandik, G., Feist, J., García-Vidal, F. J. & Schwartz, T. Cavity-enhanced energy transport in molecular systems. *Nature Materials* (2024).
- [6] Pandya, R. *et al.* Tuning the coherent propagation of organic exciton-polaritons through dark state delocalization. *Advanced Science* **9**, 2105569 (2022).
- [7] Mandal, A. *et al.* Theoretical advances in polariton chemistry and molecular cavity quantum electrodynamics. *Chemical Reviews* **123**, 9786–9879 (2023).
- [8] Blackham, L., Manjalingal, A., Koshkaki, S. R. & Mandal, A. Microscopic theory of polaron-polariton dispersion and propagation. *arXiv:2501.16622* (2025).
- [9] Tichauer, R. H., Sokolovskii, I. & Groenhof, G. Tuning the coherent propagation of organic exciton-polaritons through the cavity q-factor. *Advanced Science* **10**, 2302650 (2023).
- [10] Sokolovskii, I., Tichauer, R. H., Morozov, D., Feist, J. & Groenhof, G. Multi-scale molecular dynamics simulations of enhanced energy transfer in organic molecules under strong coupling. *Nature Communications* **14**, 6613 (2023).
- [11] Krupp, N., Groenhof, G. & Vendrell, O. Quantum dynamics simulation of exciton-polariton transport. *arXiv:2410.23739* (2024).
- [12] Ying, W., Chng, B. X. K. & Huo, P. Microscopic theory of polariton group velocity renormalization. *arXiv:2411.08288* (2024).
- [13] Liew, T. C. H. The future of quantum in polariton systems: opinion. *Opt. Mater. Express* **13**, 1938–1946 (2023).
- [14] Xiang, B. & Xiong, W. Molecular polaritons for chemistry, photonics and quantum technologies. *Chemical Reviews* **124**, 2512–2552 (2024).
- [15] Mandal, A. *et al.* Microscopic theory of multimode polariton dispersion in multilayered materials. *Nano Letters* **23**, 4082–4089 (2023).
- [16] Balasubrahmaniyam, M., Genet, C. & Schwartz, T. Coupling and decoupling of polaritonic states in multimode cavities. *Phys. Rev. B* **103**, L241407 (2021).
- [17] Sanvitto, D. & Kéna-Cohen, S. The road towards polaritonic devices. *Nature materials* **15**, 1061–1073 (2016).
- [18] Taylor, M., Mandal, A. & Huo, P. Light-matter interaction hamiltonians in cavity quantum electrodynamics. *Chemical Physics Reviews* (2025).
- [19] Keeling, J. & Kéna-Cohen, S. Bose–einstein condensation of exciton-polaritons in organic microcavities. *Annual Review of Physical Chemistry* **71**, 435–459 (2020).
- [20] Tichauer, R. H., Feist, J. & Groenhof, G. Multi-scale dynamics simulations of molecular polaritons: The effect of multiple cavity modes on polariton relaxation. *The Journal of Chemical Physics* **154** (2021).
- [21] Li, J. *et al.* Electromagnetic coupling in tight-binding models for strongly correlated light and matter. *Phys. Rev. B* **101**, 205140 (2020).
- [22] Janke, S. M., Qarai, M. B., Blum, V. & Spano, F. C. Frenkel–holstein hamiltonian applied to absorption spectra of quaterthiophene-based 2d hybrid organic–inorganic perovskites. *The Journal of Chemical Physics* **152**, 144702 (2020).
- [23] Troisi, A. & Orlandi, G. Charge-transport regime of crystalline organic semiconductors: Diffusion limited by thermal off-diagonal electronic disorder. *Physical Review Letters* **96**, 086601 (2006).
- [24] Arnardottir, K. B., Moilanen, A. J., Strashko, A., Törmä, P. & Keeling, J. Multimode organic polariton lasing. *Physical Review Letters* **125**, 233603 (2020).
- [25] Terry Weatherly, C. K., Provazza, J., Weiss, E. A. & Tempelaar, R. Theory predicts uv/vis-to-ir photonic down conversion mediated by excited state vibrational polaritons. *Nature Communications* **14**, 4804 (2023).
- [26] Litinskaya, M., Reineker, P. & Agranovich, V. Exciton-polaritons in a crystalline anisotropic organic microcavity. *Physica Status Solidi (a)* **201**, 646–654 (2004).
- [27] Frisk Kockum, A., Miranowicz, A., De Liberato, S.,

- Savasta, S. & Nori, F. Ultrastrong coupling between light and matter. *Nature Reviews Physics* **1**, 19–40 (2019).
- [28] Qin, W., Kockum, A. F., Muñoz, C. S., Miranowicz, A. & Nori, F. Quantum amplification and simulation of strong and ultrastrong coupling of light and matter. *Physics Reports* **1078**, 1–59 (2024).
- [29] Chng, B. X., Mondal, M. E., Ying, W. & Huo, P. Quantum dynamics simulations of exciton polariton transport. *Nano Letters* (2025).
- [30] Jasrasaria, D., Mandal, A., Reichman, D. R. & Berkelbach, T. C. Simulating anharmonic vibrational polaritons beyond the long wavelength approximation. *The Journal of Chemical Physics* **162** (2025).
- [31] Keeling, J. & Kéna-Cohen, S. Bose–einstein condensation of exciton-polaritons in organic microcavities. *Annual Review of Physical Chemistry* **71**, 435–459 (2020).
- [32] Antoniou, P., Suchanek, F., Varner, J. F. & Foley IV, J. J. Role of cavity losses on nonadiabatic couplings and dynamics in polaritonic chemistry. *The Journal of Physical Chemistry Letters* **11**, 9063–9069 (2020).
- [33] Qiu, L. *et al.* Molecular polaritons generated from strong coupling between cdse nanoplatelets and a dielectric optical cavity. *The Journal of Physical Chemistry Letters* **12**, 5030–5038 (2021).
- [34] Koessler, E. R., Mandal, A. & Huo, P. Incorporating lindblad decay dynamics into mixed quantum-classical simulations. *The Journal of Chemical Physics* **157** (2022).
- [35] Hoffmann, N. M., Lacombe, L., Rubio, A. & Maitra, N. T. Effect of many modes on self-polarization and photochemical suppression in cavities. *The Journal of Chemical Physics* **153** (2020).
- [36] Mandal, A. & Huo, P. Investigating new reactivities enabled by polariton photochemistry. *The Journal of Physical Chemistry Letters* **10**, 5519–5529 (2019).
- [37] Xu, J., Zhou, R., Li, T. E., Hammes-Schiffer, S. & Kanai, Y. Lagrangian formulation of nuclear–electronic orbital ehrenfest dynamics with real-time tddft for extended periodic systems. *The Journal of Chemical Physics* **161** (2024).
- [38] Li, T. E. *et al.* Mixed quantum-classical electrodynamics: Understanding spontaneous decay and zero-point energy. *Physical Review A* **97**, 032105 (2018).
- [39] Tannor, D. J. *Introduction to quantum mechanics: a time-dependent perspective* (2007).
- [40] Nielsen, M. A. & Chuang, I. L. *Quantum computation and quantum information*, vol. 2 (Cambridge university press Cambridge, 2001).
- [41] Kowalewski, M., Bennett, K. & Mukamel, S. Non-adiabatic dynamics of molecules in optical cavities. *The Journal of Chemical Physics* **144** (2016).
- [42] Hu, W., Gustin, I., Krauss, T. D. & Franco, I. Tuning and enhancing quantum coherence time scales in molecules via light-matter hybridization. *The Journal of Physical Chemistry Letters* **13**, 11503–11511 (2022).
- [43] Kar, A. & Franco, I. Quantifying fermionic decoherence in many-body systems. *The Journal of Chemical Physics* **146** (2017).
- [44] Franco, I. & Appel, H. Reduced purities as measures of decoherence in many-electron systems. *The Journal of Chemical Physics* **139** (2013).